

## COSMIC EMULATION: FAST PREDICTIONS FOR THE GALAXY POWER SPECTRUM

JULIANA KWAN<sup>1</sup>, KATRIN HEITMANN<sup>1,2,3</sup>, SALMAN HABIB<sup>1,2,3</sup>, NIKHIL PADMANABHAN<sup>4</sup>, HAL FINKEL<sup>5</sup>,  
NICK FRONTIERE<sup>1,6</sup> AND ADRIAN POPE<sup>1</sup><sup>1</sup> High Energy Physics Division, Argonne National Laboratory, Lemont, IL 60439<sup>2</sup> Kavli Institute for Cosmological Physics, The University of Chicago, Chicago, IL 60637<sup>3</sup> Mathematics and Computer Science Division, Argonne National Laboratory, Lemont, IL 60439<sup>4</sup> Department of Physics, Yale University, 260 Whitney Ave., New Haven, CT 06520<sup>5</sup> Argonne Leadership Computing Facility, Argonne National Laboratory, Lemont, IL 60439<sup>6</sup> Department of Physics, The University of Chicago, Chicago, IL 60637*The Astrophysical Journal, submitted*

## ABSTRACT

The halo occupation distribution (HOD) approach has proven to be an effective method for modeling galaxy clustering and bias. In this approach, galaxies of a given type are probabilistically assigned to individual halos in N-body simulations. In this paper, we present a fast emulator for predicting the fully nonlinear galaxy power spectrum over a range of freely specifiable HOD modeling parameters. The emulator is constructed using results from 100 HOD models run on a large  $\Lambda$ CDM N-body simulation, with Gaussian Process interpolation applied to a PCA-based representation of the galaxy power spectrum. The total error is currently  $\sim 3\%$  ( $\sim 2\%$  in the simulation and  $\sim 1\%$  in the emulation process) from  $z=1$  to  $z=0$ , over the considered parameter range. We use the emulator to investigate parametric dependencies in the HOD model, as well as the behavior of galaxy bias as a function of HOD parameters. The emulator is publicly available at <http://www.hep.anl.gov/cosmology/CosmicEmu/emu.html>.

*Subject headings:* Cosmology:  $N$ -body simulations

## 1. INTRODUCTION

Measurements of galaxy clustering at large scales provide essential cosmological information, including key inputs to investigations of dark energy, the growth rate of structure, and neutrino mass. In particular, observations of two-point clustering statistics, such as the power spectrum and correlation function of galaxies obtained from large scale structure surveys, such as the Sloan Digital Sky Survey (SDSS)/BOSS (Baryon Oscillation Spectroscopic Survey), 2dFGRS (Two-degree Field Galaxy Redshift Survey), and WiggleZ, have been of particular significance (Tegmark et al. 2004; Pope et al. 2004; Cole et al. 2005; Eisenstein et al. 2005; Tegmark et al. 2006; Parkinson et al. 2012). Some of the strongest current constraints on the nature of dark energy have been derived from measurements of the Baryon Acoustic Oscillations (BAO) peak (e.g. Anderson et al. 2012) and redshift space distortions (RSD) (e.g. Reid et al. 2012). Aside from the BAO scale, the amplitude and shape of the galaxy power spectrum (or correlation function) provides further cosmological information. In this case, it is desirable to include as many  $k$ -modes as is practical in the analysis, however, to do so requires that the nonlinear regime of structure formation be accurately modeled. As has been appreciated for quite some time, an essential difficulty is that galaxies are biased tracers of the underlying density field (Kaiser 1984; Dekel & Rees 1987). Because the nature of the bias is complex and often difficult to unravel, the underlying cosmological information cannot be straightforwardly extracted.

Modeling the distribution of galaxies remains an enduring problem in cosmology. N-body methods, while extremely successful in capturing the dark matter distribution at high resolution, do not incorporate the required baryonic physics for galaxies to emerge out of the large scale structure self-consistently. Furthermore, the positions of galaxies do not necessarily follow that of the dark matter, resulting in a nontrivial bias between statistical measurements of the clustering patterns between dark

matter and galaxies. However, as mentioned above, accurate modeling of the nonlinear distribution of galaxies is crucial for extracting cosmological information from large scale structure surveys and understanding galaxy formation. Hydrodynamic simulations are still far from attaining the required degree of maturity needed to provide a complete first-principles understanding of galaxy formation. For these reasons, a number of phenomenological approaches – varying considerably in the amount of physical input – have been employed in the continuing quest to faithfully model galaxy clustering. (For a recent review, see Baugh 2013.)

The original, and simplest, approach is to assume a (nonlinear, scale-dependent) fitting function for the bias (defined, say, as the ratio between the galaxy and the linear or nonlinear matter power spectrum), combine this with clustering measurements, and marginalize over the free parameters. Like any such general approach, the problem is that the fitting form is not necessarily based on a physically correct model for galaxy formation, and if the form itself is not sufficiently flexible, this can lead to systematic errors in the determination of cosmological parameters. (See, e.g., a comparison of results from different bias models in Swanson et al. 2010; Parkinson et al. 2012.)

More detailed models for inferring the location of galaxies can be obtained by working at the level of dark matter-dominated halos and subhalos obtained from N-body simulations. These methods fall into three main categories: Halo Occupation Distribution (HOD) modeling, Subhalo/Halo Abundance Matching (S/HAM) and Semi-Analytic Models (SAMs). The HOD model is a probabilistic description that aims to reproduce the statistical distribution of target galaxies on average. This is achieved by populating dark matter halos with galaxies as a function of the halo mass. (We discuss HOD modeling more fully in Section 2.) Halo abundance matching is an empirical procedure that involves rank ordering dark matter halos and subhalos in terms of a particular characteristic, such as

mass or peak circular velocity during its accretion history (Vale & Ostriker 2004; Conroy et al. 2006; Wetzel & White 2010; Moster et al. 2010; Guo et al. 2010). Similarly, the galaxies are ordered according to an observable feature, say, luminosity. In this example, the most massive halo would be matched to the most luminous galaxy, the next most massive halo assigned the next most luminous galaxy, and so on, until no galaxies remain. This process ensures that the luminosity function is exactly reproduced by the synthetic galaxy catalog. Semi-analytic models are the most complex, providing a simplified accounting of a large number of (baryonic) physical processes, embedded within N-body simulations. They include phenomenological prescriptions for galaxy formation and associated effects such as gas cooling, AGN and supernova feedback, and star formation, based on the subhalo and halo formation history (White & Frenk 1991; Kauffmann, White, & Guiderdoni 1993; Cole et al. 1994; Somerville & Primack 1999; Benson et al. 2003; Baugh 2006; Benson 2010).

All of these more detailed methods can make predictions for galaxy clustering (and hence for bias), by using N-body simulations and some number of observational inputs to fix modeling parameters. The results for the galaxy power spectrum or correlation functions depend on the modeling parameters, as well as on cosmology. In many cases, it is not obvious exactly how the final answer depends on the interaction of these parameters, and an exhaustive sampling of parameter space by brute force can become computationally very expensive.

The general problem of efficiently sampling cosmological parameter space and building fast (essentially instantaneous), accuracy controlled, simulation-based predictors (“emulators”) for summary statistics has been addressed via the introduction of the Cosmic Calibration Framework (CCF). The CCF is based on efficient parameter sampling strategies coupled to Gaussian Process (GP) based interpolation and a Markov chain Monte Carlo (MCMC) sampler (Heitmann et al. 2006; Habib et al. 2007). The efficiency of the CCF for reproducing highly nonlinear observables is demonstrated in the Coyote (Heitmann et al. 2010, 2009; Lawrence et al. 2010) and extended Coyote (Heitmann et al. 2013) emulators for the matter power spectrum, accurate to 1% up to  $k = 1 \text{ Mpc}^{-1}$  and 3-5% up to  $k = 8.6 \text{ Mpc}^{-1}$ , and an emulator for the halo concentration-mass ( $c-M$ ) relation (Kwan et al. 2013), accurate to 3% at  $z = 0$ .

This paper is concerned with providing a means for efficiently predicting galaxy power spectra within the HOD model, using GP-based emulation. We adopt the HOD model as a first test case for emulation of galaxy based statistics because it is simple, yet flexible, and because it is the least demanding in terms of N-body simulation requirements. Using results from a high resolution simulation, we have populated the halos with galaxies from a sampling design with a 100 different HOD models, measuring the galaxy power spectrum from each model. This process is applied to six snapshots between  $0 \leq z \leq 1$  and we perform a linear interpolation to obtain power spectra at redshifts in between these. The emulator is driven by a GP to return a galaxy power spectrum for arbitrary HOD models within the design. Sampling from the GP is a fast and accurate means of obtaining a nonlinear galaxy power spectrum without having to populate a halo catalog with a new HOD model each time.

In the following, we discuss our HOD approach, including the parameter choices, in Section 2. We describe the simulation underlying this work in Section 3 and provide some details

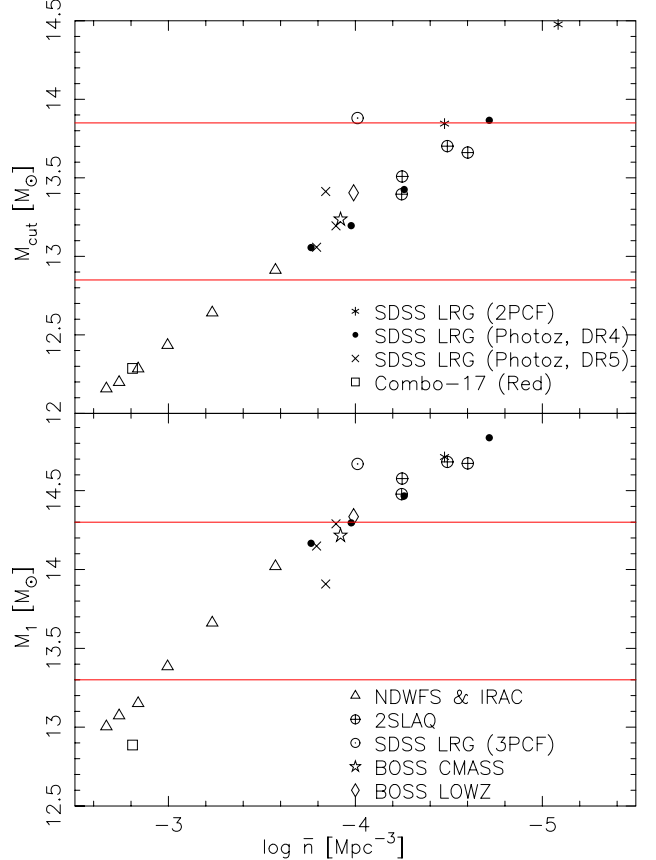


FIG. 1.— Range of the HOD emulator for  $M_{\text{cut}}$  (top panel) and  $M_1$  (bottom panel) compared to previous HOD analyses. The emulator covers the parameter space between the red lines. The survey data points are taken from Table A1 of Parejko et al. (2013) and include: Zheng et al. (2009) [SDSS LRG (2PCF)], Blake et al. (2008) [SDSS LRG (Photo-z, DR4)], Padmanabhan et al. (2009) [SDSS LRG (Photo-z, DR5)], Phleps et al (2006) [Combo-17 (Red)], Brown et al. (2008) [NDWFS & IRAC], Wake et al. (2008) [2SLAQ], Kulkarni et al (2007) [SDSS LRG (3PCF)], White et al. (2011) [BOSS CMASS] and Parejko et al. (2013) [BOSS LOWZ].

on extracting the galaxy power spectra for the different HOD models from the simulation. Section 4 describes the emulator construction itself and the tests used for verifying its accuracy. An initial set of scientific results based on the new emulator are reported in Sections 6 and 7, analyzing the dependence of the galaxy power spectrum on different HOD parameters and determining galaxy bias for different HOD models. We conclude with a short discussion in Section 8.

## 2. THE HALO OCCUPATION MODEL

The Halo Occupation Distribution model (Kauffmann et al. 1997; Jing et al. 1998; Benson et al. 2000; Peacock & Smith 2000; Seljak 2000; Berlind & Weinberg 2002) has evolved over time (Cf. Zheng et al. 2005) into a straightforward method for associating galaxies with halos. The idea behind the HOD model is that every galaxy is required to be contained within a dark matter halo and galaxy populations are split into ‘centrals’, the bright main galaxy inside the halo, located at the halo center, and surrounding dimmer ‘satellite’ galaxies. HOD models are calibrated against clustering observations of sets of target galaxies, allowing for an interpretation of the measurement in terms of a galaxy population model for halos. In this sense, the models are not predictive, and, in principle, have to be tuned to

the galaxy population (defined, e.g., by color and luminosity) under consideration. (It is also not obvious that the simple assumption of the halo mass as the master variable is sufficiently accurate, due to halo assembly bias, as discussed in Gao et al. 2005.) Despite these caveats, the HOD approach has proven to be very successful when applied to large scale structure surveys, mostly to interpret their galaxy populations. These studies have informed us about the typical host halo mass and the ratio of satellite to central galaxies for a number of galaxy populations. The HOD model has been applied to both photometric and spectroscopic galaxy surveys, and hence galaxy types, including Luminous Red Galaxies (LRGs), in the SDSS (Zehavi et al. 2004; Zehavi et al. 2005; Kulkarni et al 2007; Blake et al. 2008; Zheng et al. 2009; Padmanabhan et al. 2009) and combined 2dF-SDSS LRG and QSO survey (2SLAQ) (Wake et al. 2008), red galaxies from the NOAO Deep Wide Field Survey (NDWFS) and *Spitzer* IRAC Shallow Survey (Brown et al. 2008) and Combo-17 (Phleps et al 2006) and CMASS (White et al. 2011) and LOWZ (Parejko et al. 2013) populations from BOSS.

In order to be specific, we adopt here the HOD model of Zheng et al. (2009) for SDSS LRGs, although other models could easily be considered. In this particular case, the average number of central and satellite galaxies, in a halo of mass  $M$ , is determined by the following equations:

$$\langle n_{cen} \rangle = \text{erfc} \left( \frac{\ln M - \ln M_{cut}}{\sqrt{2}\sigma} \right), \quad (1)$$

$$\langle n_{sat} \rangle = \left( \frac{M - \kappa M_{cut}}{M_1} \right)^\alpha. \quad (2)$$

Each halo is assigned a probability of hosting a central galaxy based on the mass of the halo, with the sharpness of the cut-off mass determined by the parameter  $\sigma$ . This is enforced by choosing a random number from a uniform distribution between 0 and 1; if this number is less than  $\langle n_{cen} \rangle$ , then we place a central galaxy inside the halo.

If the halo is sufficiently massive to satisfy an additional cut in halo mass, imposed by  $\kappa M_{cut}$ , then more galaxies are placed around the halo center as satellite galaxies; how many of these are inserted into the halo is controlled by the parameter  $\alpha$ . We do not allow for halos to host satellite galaxies without a first being assigned a central galaxy. We assume that the number of satellite galaxies follows a Poisson distribution with mean  $\langle n_{sat} \rangle$ . The effect of these parameters on the mean number of galaxies assigned to each halo are illustrated in Figure 2 for two example HOD models. When placing a satellite galaxy into a halo in the simulation, a random dark matter particle belonging to the halo is drawn and the satellite galaxy assumes the position and velocity of that particle. This is because the simulations do not have sufficient mass resolution to track all relevant subhalos belonging to each halo to provide the correct number of satellite galaxies to satisfy every HOD model that we use.

The ranges of HOD parameters that we cover are given in Table 1 and illustrated in Figure 1 with respect to observational values obtained from large scale structure surveys. Figure 2 shows the values of  $\langle n_{cen} \rangle$  and  $\langle n_{sat} \rangle$  for the two HOD models at the extreme ends of the prior range. The emulator comfortably covers the HOD models used for the analysis of the recent CMASS BOSS results (White et al. 2011) as well as many SDSS LRG samples, depending on the redshift and luminosity cuts made. The ranges are determined by the mass resolution of our simulation; we only consider halos with a minimum mass

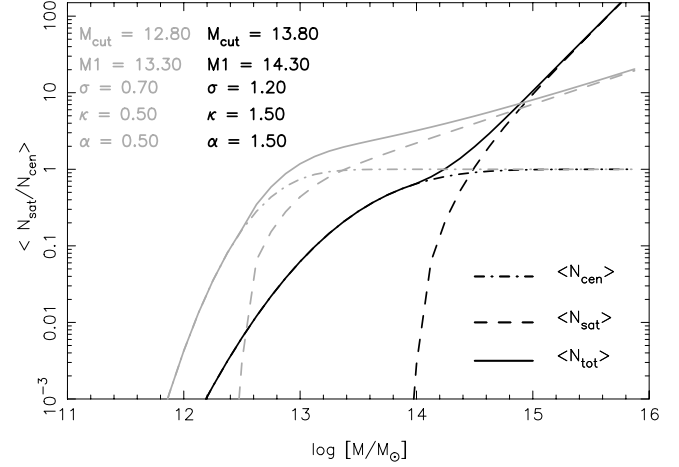


FIG. 2.— Mean number of central (dot-dashed) and satellite (dashed) galaxies per halo for two extreme HOD models within the prior ranges of the emulator. The average total number of galaxies per halo is shown as a solid curve. The two models shown have the lowest (grey) and highest (black) values in the HOD parameter space specified in Table 1.

TABLE 1  
PRIOR RANGE OF HOD MODEL PARAMETERS

12.85	$\leq \log_{10}(M_{cut}[M_\odot]) \leq$	13.85
13.3	$\leq \log_{10}(M_1[M_\odot]) \leq$	14.3
0.5	$\leq \sigma \leq$	1.2
0.5	$\leq \kappa \leq$	1.5
0.5	$\leq \alpha \leq$	1.5

cut set by a lower limit of 40 particles per halo, this in turn imposes a lower limit on  $M_{cut}$  and  $\sigma$ . While the smallest halos that we populate are actually less massive than the value of  $M_{cut}$  in that HOD model because  $\sigma$  can substantially increase the value of  $\langle n_{cen} \rangle$  for low mass halos, we have ensured that these limits are within the mass resolution of our simulation (discussed below) by setting an appropriately conservative lower limit on  $M_{cut}$ . The upper limit is set mainly by statistical limitations due to the finite number of high mass halos in the simulation – a lower mass cut reduces the amount of noise in the power spectrum, and is in accordance with current and future galaxy surveys. Galaxy samples with excessively high  $M_{cut}$  and  $M_1$  will have a low number density (high mass halos are rare) and as such there are few surveys that will target such galaxies. We have checked that the limits imposed in Table 1 will introduce an error of 1.5% at most, for models at the lower edge of the design, due to the missing low mass halos in the simulation.

### 3. N-BODY SIMULATIONS

Our HOD catalogs are based on an N-body simulation with a box-size of  $L = 2100$  Mpc,  $3200^3$  simulation particles and a cosmology similar to WMAP7:  $\Omega_m = 0.2648$  (including both cold dark matter and baryonic matter),  $\Omega_b = 0.0448$ ,  $n_s = 0.963$ ,  $\sigma_8 = 0.8$ , and  $h = 0.71$ . This leads to a particle mass,  $m_p = 1.05 \cdot 10^{10} M_\odot$ . The force resolution was set to  $\sim 9$  kpc. Initial conditions were set with the Zel'dovich approximation, at  $z_{in} = 200$ . The simulation was performed using the HACC (Hardware/Hybrid Accelerated Cosmology Code) framework (Habib et al. 2009; Pope et al. 2010; Habib et al. 2012) on the Mira supercomputer at the Argonne Leadership Computing Facility. To demonstrate the extent of finite volume effects on the power

spectrum, in Figure 3 we show the matter power spectrum compared to the extended Coyote emulator (Heitmann et al. 2013), which is accurate to 3%. To avoid finite sampling errors on the very largest scales, we only consider modes with  $k > 0.03 \text{ Mpc}^{-1}$  in the simulation, as indicated by the vertical line.

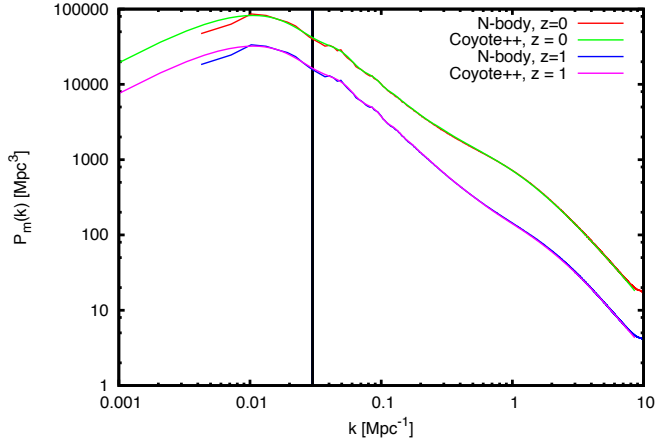


FIG. 3.— Matter power spectrum from the N-body simulation at  $z = 0$  and at  $z = 1$ . The extended Coyote emulator (Heitmann et al. 2013) results are overplotted for comparison. The black vertical line indicates the scale at which we start fitting the N-body power spectrum to perturbation theory (discussed in Section 4.2)

Halos were identified with a Friends-of-Friends (FOF) algorithm (Einasto et al. 1984; Davis et al. 1985). This algorithm groups all particles that are joined to at least one other particle by a certain link length,  $b$ , as belonging to the same halo; approximately equivalent to requiring a minimum isodensity contour before an overdensity is considered a halo. We chose to use  $b = 0.168$ , since this in rough correspondence with a spherical overdensity mass of  $M_{200}$ , reduces halo over-linking, and is also consistent with other HOD analyses carried out on recent measurements, e.g. by White et al. (2011) and Parejko et al. (2013). The last feature allows for an easy comparison of results. The smallest halos we consider have at least 40 particles, leading to a halo mass of  $\sim 4.2 \cdot 10^{10} \text{ M}_\odot$ . At  $z = 0$ , we have a total of  $\sim 3.4 \cdot 10^7$  halos in the simulation and there are  $\sim 2000$  halos with masses  $> 9.55 \cdot 10^{14} \text{ M}_\odot$ , ensuring good statistics for massive halos.

### 3.1. Measuring the Galaxy Power Spectrum from N-body Simulations

After having identified the halos in the simulations, the next step is the generation of galaxy catalogs following our HOD prescription outlined in Section 2. Varying the set of five HOD parameters introduced in Table 1, we generate 100 different models, arranged in a space-filling Symmetric Latin Hypercube design as explained in more detail in Section 4.1. For each of the 100 HOD models, the halo catalog is populated with galaxies from which we then measure a galaxy power spectrum. The power spectrum is defined as:

$$P(k) = \langle |\delta(k)|^2 \rangle, \quad (3)$$

where  $\delta = (\rho - \bar{\rho})/\bar{\rho}$  and because we are interested in characterising the clustering of galaxies,  $\rho$  is the density of the galaxy field in the Universe. We use a Cloud in Cell (CIC) deposition on to a  $2048^3$  grid to generate the density field, followed by a standard power spectrum estimation step using the Fast Fourier Transform (FFT).

## 4. EMULATING THE GALAXY POWER SPECTRUM

Building a prediction scheme, or emulator, for the galaxy power spectrum, proceeds in three steps: (i) the design step, where we decide the HOD parameter settings at which to generate galaxy power spectra, (ii) a smoothing step, where we take the resulting power spectra and filter discreteness noise caused by the finite number of galaxies in our catalogs, (iii) the interpolation step, where we build a Gaussian Process model to generate predictions at new points in the HOD parameter space, leading to the final emulator. Next, we describe each of these steps in detail, followed by a rigorous testing procedure to verify the accuracy of our new emulator.

### 4.1. Design Strategy

The distribution of models in the five dimensional HOD parameter space – the emulator design – is determined by a Symmetric Latin Hypercube to cover the maximum amount of parameter space with the fewest models. The technique for generating such a design is detailed in Heitmann et al. (2009) (including many references); the basic premise is that it is a space-filling design such that in any given two-dimensional projection of the full five-dimensional space, the models are approximately evenly sampled. We use a set of 100 HOD models that span the range given in Table 1. The number of models chosen to cover the parameter space is determined by performing a series of tests in which we vary the number of design points used from 25, 50, to 100 and build a toy emulator for each set using halo model predictions for the HOD power spectrum as a proxy model (see Cooray & Sheth 2002, for example) because these can be generated quickly. According to the halo model, the galaxy power spectrum is given by:

$$P_{\text{gal}}(k) = P_{\text{gal}}^{1h}(k) + P_{\text{gal}}^{2h}(k); \quad (4)$$

and

$$P_{\text{gal}}^{1h} = \int n(m) \frac{\langle N_{\text{gal}} (N_{\text{gal}} - 1) |m\rangle}{\bar{n}} |u(k|m)|^2 dm \quad (5)$$

$$P_{\text{gal}}^{2h} = P_L \left[ \int n(m) b(m) \frac{\langle N_{\text{gal}} |m\rangle}{\bar{n}} u(k|m) dm \right]^2, \quad (6)$$

where  $n(m)$  is the halo mass function,  $\bar{n}$  is the mean density of galaxies and  $u(k|m)$  is the dark matter mass profile in Fourier space,  $P_L(k)$  is the linear matter power spectrum and  $b(m)$  is the bias. Since there exist analytic prescriptions or fitting formulae for many of these terms, we can calculate these quantities much more readily than galaxy catalogs from N-body simulations. The accuracy checks on these toy emulators are shown in Figure 4, in which we have selected five models not included in any of the designs and compared the predictions from each emulator to these. We found the emulator easily achieves sub-percent level accuracy with only 100 models. The response surface can be more complicated in the fully nonlinear case than in the simplified proxy model. For this reason, we chose a 100 model design to assure percent level accuracy in the final product. This estimate of the accuracy is verified by our later *a posteriori* tests (Section 4.4) carried out on the full emulator.

### 4.2. Smoothing the power spectrum

In this section, we discuss the smoothing process used to convert the power spectra into noise-free estimates suitable for emulation. The galaxy power spectra generated from the simulation contain measurement noise, because of finite volume

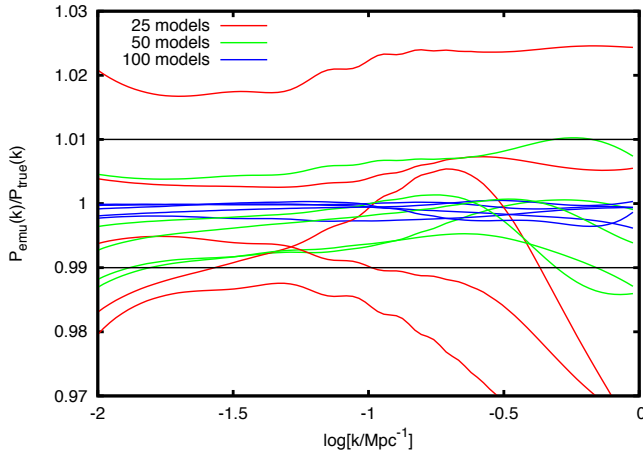


FIG. 4.— Accuracy test on the toy emulators built from halo model proxies. The aim is to estimate the number of models needed to cover the space of five HOD parameters with percent level accuracy. We built three emulators based on linear theory HOD models with 25 (red), 50 (green) and 100 (blue) design points and use these to predict the power spectrum of five models not included in the designs, which we denote  $P_{true}(k)$ . The black lines denote our targeted accuracy of 1%.

effects and discrete sampling of Fourier modes. For the GP to function properly, we do not want to model noisy estimates of quantities as this would interfere with the ability of the GP to smoothly vary across the parameter space because of the random noise included with each function. Therefore we smooth the power spectra before they are used to condition the GP. We require that this effective filtering introduces errors of no more than  $\sim 1\%$  percent into the power spectrum measurement.

Our process for smoothing the power spectrum proceeds in the following steps:

1. Transform the power spectra to  $\mathcal{P}(k) = P_{gal}(k)k^{1.5}/(4\pi^3)$  and re-bin; Lawrence et al. (2010) found that this transformation helps to enhance the baryon oscillation features. We then collect the measurements into wider bins in  $k$ . The original bin spacing of the power spectrum measured from the simulations is  $\delta k = L/N_{FFT}$ . The new bins are spaced such that there are at least 5-20 points contributing to each bin, depending on the amount of variance in the power spectrum. The difference between these power spectra is shown in Figure 5, which also demonstrates that the binning process is unbiased.
2. Perform a basis spline on the binned power spectra. We use a basis spline of order 4 with 10 coefficients evenly spaced throughout the  $k$ -range. This captures the broadband shape and provides a reasonably smooth estimate of the power spectrum for  $k > 0.1 \text{ Mpc}^{-1}$ .
3. Use perturbation theory to cover the large scale regime. Since the basis spline suppresses some of the BAO structure and the simulation does not exactly capture the wiggles due to its finite volume, perturbation theory is used to compute the the large scale power. We use one-loop perturbation theory with resummed bias parameters (McDonald 2006a,b) for the (biased) galaxy power

spectrum,  $P_{gal}(k)$ , as follows:

$$P_{gal}(k) = b_1^2 P_m(k) + \frac{1}{2} b_1^2 b_2^2 \int \frac{d^3 \mathbf{q}}{(2\pi)^3} P_m(q) [P_m(|\mathbf{k} - \mathbf{q}|) - P_m(q)] + 2b_1^2 b_2 \int \frac{d^3 \mathbf{q}}{(2\pi)^3} P_m(q) P_m(|\mathbf{k} - \mathbf{q}|) J_s^{(2)}(\mathbf{q}, \mathbf{k}) + N, \quad (7)$$

where  $P_m(k)$  is the matter power spectrum (here provided by the original Coyote emulator) and the function,

$$J_s^{(2)}(\mathbf{k}_1, \mathbf{k}_2) = \frac{5}{7} + \frac{1}{2} \frac{\mathbf{k}_1 \cdot \mathbf{k}_2}{k_1 k_2} \left( \frac{k_1}{k_2} + \frac{k_2}{k_1} \right) + \frac{2}{7} \left( \frac{\mathbf{k}_1 \cdot \mathbf{k}_2}{k_1 k_2} \right)^2. \quad (8)$$

We use publicly available code in the Cosmology Routine Library<sup>1</sup> to evaluate the integrals in Eq. 7. The bias factors,  $b_1, b_2$ , and  $N$ , cannot be predicted accurately from perturbation theory, so we perform an MCMC fit for the most likely values, using a covariance matrix calculated using the method of Tegmark (1997). Since we keep to linear scales only in this part of the smoothing procedure, the use of this covariance matrix should be sufficient. Moreover, we have demonstrated in Figure 3 that the modes we use are not substantially affected by finite volume effects, since we only use modes from  $0.03 < k < k_{max} \text{ Mpc}^{-1}$ , where  $k_{max} \in [0.12, 0.15] \text{ Mpc}^{-1}$ ; if the reduced  $\chi^2 \gg 1$ , we lower the value of  $k_{max}$  until an acceptable reduced  $\chi^2$  is found.

4. Differentiate the nonlinear power spectrum using a low-noise fifth-order Lanzcos differentiator to estimate the locations of the BAO peaks. These are needed to check that the joining process (described below) does not destroy the structure of the peaks. The Lanzcos derivative of a function  $f(x)$  is defined as:
5. Join the two halves of the power spectrum – perturbation theory informed by N-body simulations on large scales and the basis splined N-body measurements on small scales – by allowing the  $k$  value of the join to slide freely between the third and fourth BAO peak, which set the endpoints of the joining region. We match the amplitudes and first derivatives of these power spectra to ensure a smooth transition.
6. Error control test. We require that the join introduces a deviation of a few percent over the joining region to be acceptable. If the match is found to be unacceptable, perhaps because the posterior was poorly sampled or the placement of the joining region was too far into the nonlinear regime for this HOD model, the procedure is repeated from Step 3, while narrowing the range to more conservative, larger scales. The smoothness of the resulting join is demonstrated in Figure 6.

In Figure 6, we show an example HOD power spectrum with parameters,  $M_{cut} = 13.7086$ ,  $M_1 = 13.4515$ ,  $\sigma = 0.6061$ ,  $\kappa =$

<sup>1</sup>URL – <http://www.mpa-garching.mpg.de/~komatsu/crl/>

0.9444 and  $\alpha = 1.1364$ , obtained after applying all the steps in the smoothing process. This model is actually one of the most highly biased models in our HOD parameter space and therefore the most difficult model to fit using perturbation theory. The results shown in the figure demonstrate that visually, there are no discernible defects in the galaxy power spectrum caused by our smoothing procedure.

The main sources of error introduced into the smooth power spectrum originate in the fitting process. There is some width of acceptable values for  $b_1, b_2$  and  $N$  corresponding to the  $1\sigma$  confidence limit. However, the tests in Section 4.4 show that our procedure is consistent to the percent level, as we shall see in Figure 7. Briefly, the predictions of the emulator for models not included in the design cannot be accurate to 1%, if there was a substantial level of error in the best fitting values for the bias parameters.

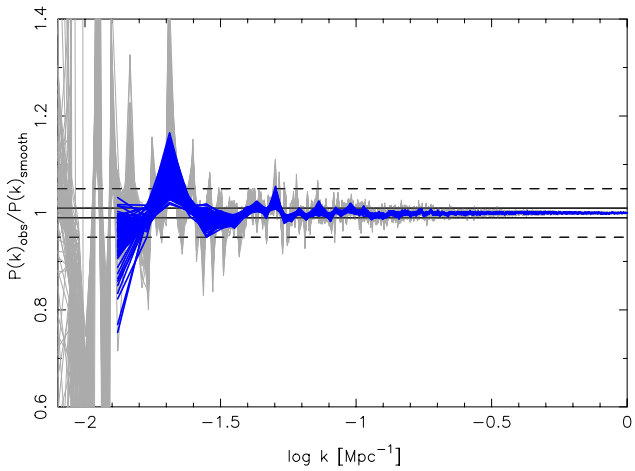


FIG. 5.— Ratio of the smoothed  $P_{gal}(k)$  to the binned  $P_{gal}(k)$  (blue) and the original  $P_{gal}(k)$  (grey) for all 100 HOD models at  $z = 0$ . The black lines are set at 1% (solid) and 5% (dashed) deviations. No obvious features from a mismatch between perturbation theory and the N-body power spectrum are visible.

### 4.3. Gaussian Process Modeling

Once the smoothed galaxy power spectra have been obtained at the design points, a Gaussian process model is conditioned on these results, and can be interrogated to provide power spectrum predictions for any set of parameters chosen to lie within the prior range of Table 1.

The GP is a family of non-parametric, Gaussian distributed functions about a set of input points. The GP returns a function whose behavior is obliged to satisfy the input points at high accuracy. Our Gaussian model exists in parameter space not in  $k$ -space; i.e. the GP does not model each point in  $k$  individually but rather the function as a whole over the entire parameter set. Overfitting is avoided by supplying a covariance function that regulates the complexity or ‘smoothness’ of the resultant function. This is achieved by controlling the relationship between each model in parameter space in terms of a distance metric. It is important that the underlying response surface mapped by the GP varies smoothly with the parameters – this requires the absence of sudden discontinuities as we

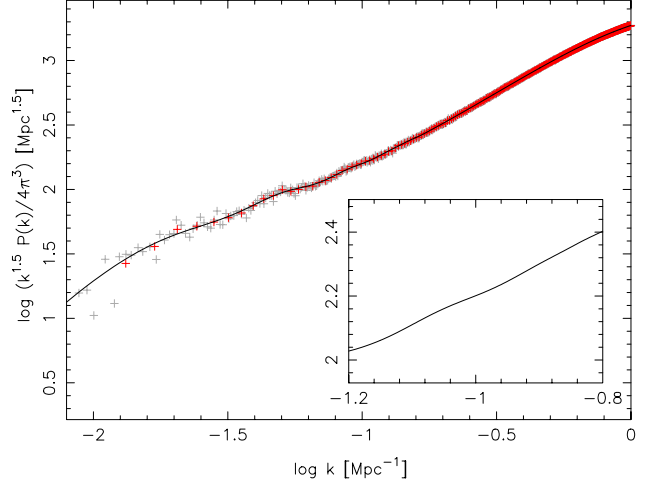


FIG. 6.— Example HOD power spectrum plotted as  $\mathcal{P}(k) = P(k)k^{1.5}/4\pi^3$ . Gray points come from the original  $P(k)$  measured from the N-body simulation, red points are the more aggressively binned data points described in Step 1 and the black line is the resultant smooth  $P(k)$ . In the insert, we have zoomed in on the joining region,  $\log(k/\text{Mpc}^{-1}) \sim -1$ , where the perturbation theory  $P(k)$  is joined onto the N-body splined  $P(k)$ .

move from one model to another with similar parameters. In most cosmological applications, this is not an issue, as most two-point statistics are quite well behaved when the underlying parameters are changed. However, we often do not know in advance the exact dependencies and degeneracies that exist in parameter space, particularly if the problem is nonlinear. For this reason, the form of the covariance function is parameterized with a set of hyperparameters. These are determined by maximizing the likelihood, which we carry out via a Markov chain Monte Carlo (MCMC) process.

Our procedure for setting up the GP closely follows the method outlined in Heitmann et al. (2006), Habib et al. (2007) and Heitmann et al. (2009). We will only briefly summarize the process here, because we are not so much concerned with the use of GPs for precision cosmology, but the application of GPs to the particular problem at hand. We refer the interested reader to the earlier papers for further details.

We first calculate the average,  $\mu(k)$ , and standard deviation,  $\sigma$ , of the set of 100 HOD power spectra and then use these to normalize each individual power spectrum, such that the resultant set of power spectra have a mean of 0 and a standard deviation of 1. To capture the features of these functions as they vary across the HOD parameter space, we decompose each power spectrum into five principal components (PCs) to reduce the dimensionality of the problem, as in Heitmann et al. (2009). We found that the five PCs were sufficient to capture over 99.999% of the variability of the power spectra in our HOD parameter space. The product of the emulator is actually the weight on each PC  $w_i$ , which is then summed as follows:

$$P_{gal}(k) = \mu(k) + \sigma \sum_{i=1}^5 \phi(k) w_i(\theta), \quad (10)$$

where  $\theta$  represents the set of HOD parameters in the design,  $\phi$  are the functions from the PC basis and  $\mu(k)$  is the mean power spectrum averaged over all 100 HOD models. For the Gaussian Process to account for the relationships between the

models that cover the parameter space, we need to specify a covariance function. Our choice for the covariance function,  $\Sigma_{l;ij}$ , is a squared exponential given by

$$\Sigma_{l;ij} = \lambda_l \prod_{k=1}^5 \rho_{kl}^{4(\theta_{ik} - \theta_{jk})^2}, \quad (11)$$

where the  $l$  index refers to the set of PCs and the  $i, j$  and  $k$  indices run over the five HOD parameters. The hyperparameters  $\lambda_l, \rho_{kl}$  and  $\lambda_p$  are set via an MCMC process and this conditions the GP. The form of the likelihood is given in Eq. B17 in Heitmann et al. (2009). One  $\lambda_l$  for each PC tunes the precision, while  $\rho_{kl}$  encodes the strength of the dependency of the  $l$ -th PC on the  $k$ -th HOD parameter. Values of  $\rho_{kl}$  that are close to unity imply a stronger relationship than values close to zero. The hyperparameter  $\lambda_p$  controls the accuracy of the projection from the original 100 model design space onto the PC basis.

Subsequent draws from the GP use the best fitting values for the hyperparameters as determined during the conditioning process. Once the GP is fully specified, we can draw a function, constrained to pass through the design points, at any point in the parameter space that satisfies the covariance function. The most computationally expensive process in generating the prediction is the calculation of the inverse of the covariance matrix with the new model included.

#### 4.4. Testing the Emulator

In this section, we test the accuracy of the emulator by comparing the power spectrum generated by the emulator to HOD models directly sampled from our N-body simulation but not included in the emulator. We apply the same smoothing process, described in Section 3.1, to these new HOD models. We repeat this test on the  $P_{gal}(k)$  emulator at each of the six redshift slices used to construct the emulator. In Figures 7 and 8, we show the results of two of these at  $z = 0$  and  $z = 1$ , respectively, demonstrating that the emulator is accurate to  $\sim 1\%$  over the range  $0.01 < k < 1 \text{ Mpc}^{-1}$ . Furthermore, the other redshifts were also verified to be accurate to  $\sim 1\%$ . Our test models are chosen to span the full range of parameters and we have set each parameter to be 10, 25, 50, 70, 90% of the width of the design. For example, the HOD model with parameters  $M_{cut} = 12.95, M_1 = 13.4, \sigma = 0.57, \kappa = 0.6$  and  $\alpha = 0.6$  has parameters set at 10% of the range of our HOD parameter space. Generally, the emulator should perform better near the center of the design and worse at the edges of the Latin hypercube, simply because there are a limited number of models that support the design edge. However, this does not seem to affect our HOD emulator because the error is dominated by the smoothing process. Note that the error in Figure 7 is percent level in the fully non-linear case rather than below sub-percent level in Figure 4 because of the additional contributions to the error budget in smoothing.

Figures 7 and 8 also show that the smoothing procedure described in Section 4.2 is consistent in reproducing the same smooth power spectrum as the emulator at least to the percent level. That is, if there was an element of stochasticity in the smoothing process, perhaps brought about by the jitter of best fitting parameters in the MCMC process, it can not be more than 1%.

The small feature near  $\log_{10}(k/\text{Mpc}^{-1}) = -0.8$  in Figures 7 and 8 is the result of the transition between perturbation theory and the smoothed nonlinear power spectrum. The feature is

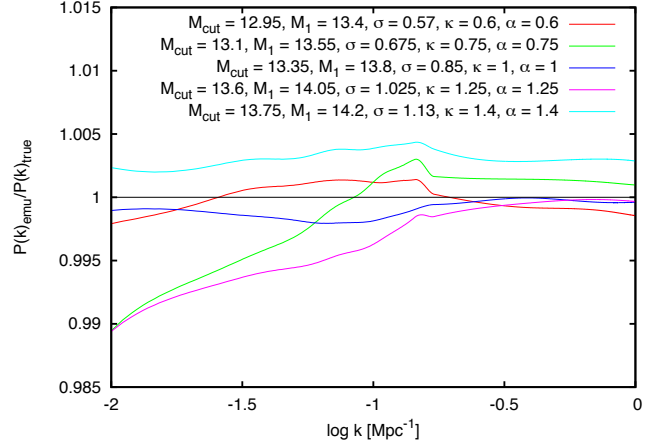


FIG. 7.— Accuracy test for  $P_{gal}(k)$  at  $z=0$ : HOD power spectrum returned by the emulator compared to one directly measured from the N-body simulation. We show five test cases in this plot, distributed throughout the design space in steps corresponding to 10 (red), 25 (green), 50 (blue), 75 (magenta), 90 (cyan)% of the full parameter range. The HOD power spectra returned by the emulator are within  $\sim 1\%$  of the smoothed N-body results on the scales  $0.01 < k < 1 \text{ Mpc}^{-1}$  for the models tested.

only present at the sub-percent level, which confirms that our process of joining the two power spectra is robust.

In addition, we have also checked the accuracy of the emulator at redshifts other than the six at  $z = 0, 0.101, 0.242, 0.434, 0.656, 1.006$  that were built into the emulator. To calculate the power spectra at other redshifts, we perform a linear interpolation over the redshifts at which the power spectra were measured. Using a snapshot at  $z = 0.53$ , we built an HOD catalog that was not incorporated into the design, measured the power spectrum and smoothed it according to the procedure described in Section 4.2. We then compared this power spectrum to one produced by the emulator and found a deviation of at most 2% when we calculate the ratio of these power spectra. This error would include both the smoothing error and the error in the emulator, because the HOD model was not a part of the design.

Considering that there is a  $\sim 2\%$  error in smoothing the power spectra and a  $\sim 1\%$  error in the emulator, we estimate the final precision of the HOD power spectra to be  $\sim 3\%$  at all redshifts considered.

## 5. COMPARISON TO ANALYTIC MODELS

We now compare the accuracy of our emulator to analytic predictions of the HOD power spectrum. These models are based on summing the 2-halo and 1-halo contributions to the galaxy power spectrum. The relevant equations for the most basic halo model, which is described in Cooray & Sheth (2002) are listed in Section 4.1 (equation 4 – 6). The 2-halo term (Eqn 5) describes galaxy pairs in two different halos, while the 1-halo term (equation 6) arises from the galaxy pairs that occupy the same halo. There have been many revisions to this model and we consider one of the most popular, the Zheng (2004) model, which we will call Z04, with some recent revisions by Tinker et al. (2010). There are four ingredients to this model: the halo profile, the concentration-mass relation, the large scale halo bias and the halo mass function. When-

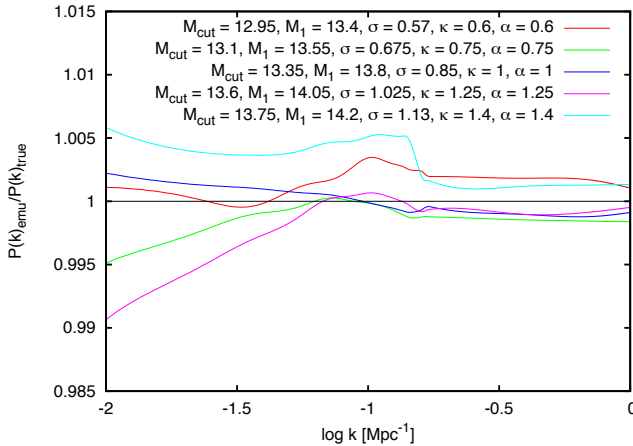


FIG. 8.— Accuracy test for  $P(k)$  at  $z = 1$ . As in Figure 8, we test the emulator against five new HOD models drawn from the N-body simulation that were not included in the original design.

ever possible, we take the the most recent fitting functions that are the most widely accepted in the literature to model these four quantities. We use a NFW profile to describe the distribution of galaxies in a halo. For the concentration-mass relation, we use Bhattacharya et al. (2013), which was calibrated on a  $\Lambda$ CDM cosmology that closely resembles our simulation in its  $\Omega_m$  and  $\sigma_8$  values.

To model the large scale halo bias, we use the following fitting function from Tinker et al. (2010)

$$b(\nu) = 1 - A \frac{\nu^a}{\nu^a + \delta_c^a} + B\nu^b + C\nu^c \quad (12)$$

where  $A = 1 + 0.24y\exp{[-(4/y)^4]}$ ,  $a = 0.44y - 0.88$ ,  $B = 0.183$ ,  $b = 1.5$ ,  $C = 0.019 + 0.107y + 0.19\exp{[-(4/y)^4]}$ ,  $c = 2.4$  and  $y = \log_{10}\Delta$  and  $\Delta = 200$ . For our FOF catalogues with  $b = 0.168$ ,  $\Delta = 200$  is the most appropriate overdensity value considered in Tinker et al. (2010), who used halo catalogues identified with a spherical overdensity (SOD) finder. Indeed, Tinker et al. (2010) reports that a good agreement was found in the measured values of the large scale bias between FOF halo catalogues with  $b = 0.168$  and a SOD catalogue of  $\Delta = 200$ , despite the differences in the methodology and effects of aspherical FOF halo isodensity contours (Lukic et al 2007).

Since we use a linking length of  $b = 0.168$  to construct our galaxy catalogues, we are unable to use a fitting function for the universal form for the mass function, which is calibrated on  $b = 0.2$ . Instead, we use the FOF halo mass function directly measured from our simulation.

To improve the accuracy of the model on small scales in comparison to N-body simulations, the Z04 model contains an additional modification that imposes halo exclusion by setting the upper integration limit,  $M_{lim}$ , on the 2-halo term to avoid counting contributions from two overlapping halos. This is done by requiring  $M_{lim} = 4/3\pi(r/2)^3\rho_c\Omega_m\Delta$ , where  $r$  is the radius of the halo, such that no other halo residing within half of the radius of a halo of mass,  $M_{lim}$ , can be considered.

In Figure 9, we compare the Z04 model, calculated with the halo model components described above, against our HOD emulator. We chose a random set of model parameters within

our parameter range and because of halo exclusion in the Z04 model, to make the comparison fair, we plot the power spectrum from the emulator with and without Poisson shot noise subtraction. On large scales, the amplitudes of the power spectra agree to  $\sim 3\%$  but begin to deviate at  $k \sim 0.1\text{Mpc}^{-1}$  as the scale dependent bias becomes important and the 1-halo term becomes inadequate.

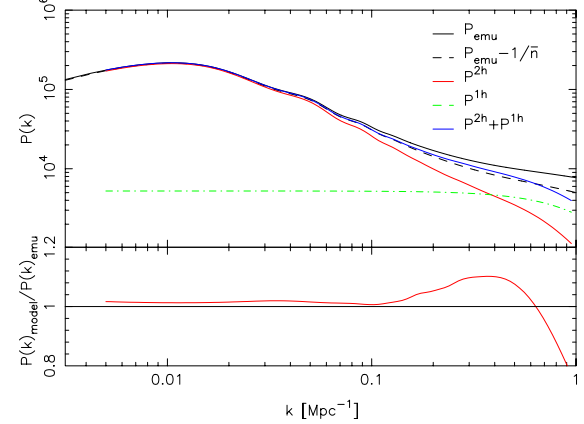


FIG. 9.— The power spectrum from HOD emulator, with and without Poisson shot-noise (solid and dashed black, respectively) compared to the Zheng et al analytic model. We have split the total power spectrum from the Zheng model (solid blue) into its 2-halo (solid red) and 1-halo (dashed green) components. The large scale bias is modelled quite well at the  $\sim 3\%$  level up to  $k \sim 0.1 \text{ Mpc}^{-1}$ , but then there are deviations of 10-20% on smaller scales (bottom panel).

Past this scale, the Z04 model can no longer be trusted to derive accurate constraints on cosmology or the HOD parameters as the shape of the power spectrum is significantly biased at the 10-20% level. Unfortunately, this sort of halo model approach is only as good as its constituent fitting functions and the accuracy of these may be severely restrictive and dependant on the cosmology, volume, mass resolution etc. of the simulations used to calibrate them.

Nonetheless, these models give an intuitive understanding of the HOD power spectrum via the halo model and its 2-halo and 1-halo contributions. Furthermore, while undoubtedly more accurate, the emulator is restricted to operate within a certain parameter range, while the halo model is essentially unrestricted.

## 6. PARAMETER SENSITIVITIES

Now that we are in possession of an HOD emulator, we can smoothly vary each HOD parameter in turn to investigate parametric degeneracies and other effects on the galaxy power spectrum. In Figure 10, we explore the effect of changing each parameter on the galaxy power spectrum. We divide the parameter space into ten evenly spaced bins for each HOD parameter in turn, while keeping all the other parameters fixed at the center of the design, i.e.  $M_{cut} = 13.35, M_1 = 13.8, \sigma = 1, \kappa = 1$  and  $\alpha = 1$ . The resultant power spectra are plotted in Figure 10.

Figure 10 shows that the parameters that most strongly affect the HOD power spectrum are  $M_{cut}$  and  $\alpha$ , while  $\kappa$  only minimally affects the power spectrum over our parameter range. The parameter,  $M_{cut}$ , has the greatest influence in determining which halo will host a central galaxy. Since the majority of

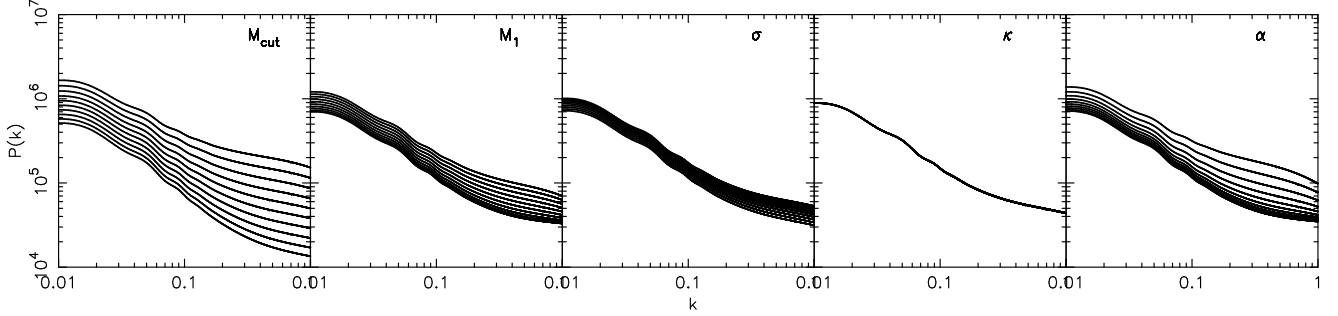


FIG. 10.— Emulated galaxy power spectrum at  $z = 0$ . The five HOD parameters  $M_{cut}$ ,  $M_1$ ,  $\sigma$ ,  $\kappa$  and  $\alpha$  are varied. A single parameter is changed at a time in each panel, while the other four parameters are kept fixed at the midpoint of the parameter space. We divide the range of each parameter into ten evenly spaced bins, these are the values fed into the HOD emulator.

galaxies in our HOD models are centrals, it follows that  $M_{cut}$  has the greatest effect on the HOD power spectrum, especially on the linear bias. In Figure 11, we calculate  $\partial \log P(k) / \partial \theta_i$ , where  $\theta_i = \{M_{cut}, M_1, \sigma, \kappa, \alpha\}$  to demonstrate the degeneracies between the HOD parameters. All the parameters are degenerate on large scales, since they all show a similar relationship with  $k$  up to  $k = 0.05 \text{ Mpc}^{-1}$ . This implies that they are all capable of shifting the linear, large scale asymptotic bias; but higher  $M_{cut}$  and  $\alpha$  values will increase the bias as the galaxy catalog will be populated from higher mass halos and more satellite galaxies, whereas increasing  $M_1$  will decrease the bias, as a catalog with a higher  $M_1$  will contain fewer satellite galaxies, if all other parameters are kept fixed. The parameter,  $\sigma$ , widens the mass cut on the central galaxies to accept more low mass halos and increasing  $\sigma$  reduces the linear bias. At smaller scales up to  $k = 1 \text{ Mpc}^{-1}$ ,  $M_{cut}$  affects the shape of the HOD power spectrum more strongly than any other parameter. At these scales, the power spectrum is still dominated by the two-halo term, so the additional satellite galaxies produced by having a larger value of  $\alpha$  contributes less clustering than does  $M_{cut}$ . As in Figure 10,  $\kappa$  does very little to change the shape of the power spectrum. We have also investigated these relationships at  $z = 0.5$  in Figure 11. By this redshift, the number of massive halos has been greatly reduced compared to  $z = 0$ . This reduces the influence of  $M_1$  and  $\alpha$  on the HOD power spectrum, which are only active parameters if  $M \gtrsim 10^{14} M_\odot$ . Conversely,  $\sigma$  and  $M_{cut}$  become more influential at higher redshift.

Our results agree with Parejko et al. (2013), who found similar dependencies on the shape of the projected HOD correlation function,  $w_p$ , although their study probes much smaller scales than our HOD power spectrum emulator.

## 7. NONLINEAR BIAS

We now investigate the nonlinear galaxy bias with our HOD emulator. This is a difficult quantity to model analytically beyond the large scale, linear limit and our emulator offers a means of easily accessing nonlinear predictions for the galaxy bias. We define the galaxy bias as follows:

$$b(k) = \sqrt{\frac{P_{gal}(k)}{P_m(k)}}, \quad (13)$$

where  $P_m(k)$  can be derived from either the linear or nonlinear matter power spectrum. In Figures 12 and 13, we show the evolution of the galaxy bias as a function of scale at  $z = 0$  and  $z = 1$ , respectively. As in Figure 10, we have divided the parameter range into 10 bins, but in this section, we allow only

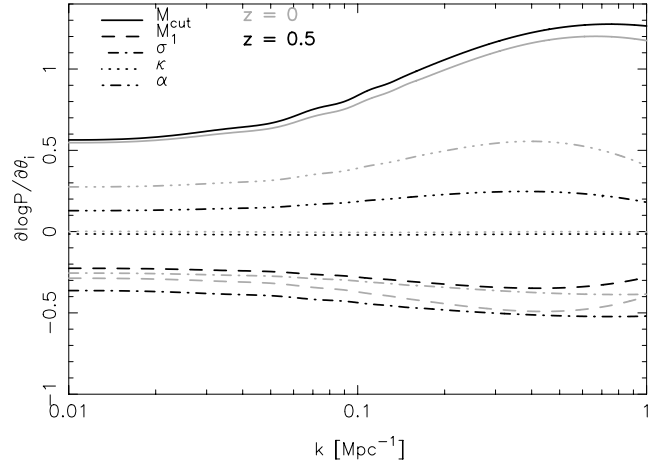


FIG. 11.— Derivatives of the power spectrum with respect to the 5 HOD parameters,  $\theta_i = \{M_{cut} \text{ (solid)}, M_1 \text{ (dashed)}, \sigma \text{ (dot dashed)}, \kappa \text{ (dotted)} \text{ and } \alpha \text{ (dot-dot dashed)}\}$ . We compute each partial derivative at the midpoint of the design at two redshifts,  $z = 0$  (grey) and  $z = 0.5$  (black).

$M_{cut}$  to change, since this is the parameter that the HOD power spectrum is most sensitive to, as shown in Section 6.

Figures 12 and 13 show that the nonlinearity of the bias increases with redshift when the HOD model is kept the same. The scale dependence of the bias in relation to the nonlinear matter power spectrum is quite moderate for the models with a low  $M_{cut}$  and is approximately linear until  $k \sim 0.1 - 0.2 \text{ Mpc}^{-1}$ . The scale dependence is stronger at higher redshift, but this is because a galaxy catalog at this redshift with the same HOD parameters will contain rarer halos, i.e. there were much fewer  $10^{15} M_\odot$  halos at  $z = 1$  than  $z = 0$  and so these are more biased with respect to the matter density field.

In evaluating power spectra where the density field is reconstructed from mass points, there is an unavoidable shot noise contribution due to the finite mass resolution. At the highest  $k$  values considered here, the shot noise in the matter power spectra is insignificant, because the particle Nyquist wave number in the simulation is sufficiently large (see Heitmann et al. 2010, for detailed tests). A similar situation exists for the galaxy field: the preferential sampling of halos amongst the dark matter distribution introduces an element of shot noise in the galaxy power spectrum. Halos are biased tracers that tend to follow the highest peaks of dark matter density field, and by placing galaxies inside these, we have inherently chosen positions that are not a fair sample of the entire density field and so the generation of

shot noise is not entirely a Poisson process in the galaxy power spectrum. For a given survey, the discreteness is determined by the galaxy density (selection function), and is a physical effect. In principle, one can attempt to model this contribution or filter it, but we choose not to do so here. (A naive Poisson noise subtraction will most likely introduce systematic error into the emulator.) It is important to note that the galaxy shot noise will make a substantial contribution to the bias shown in Figures 12 and 13.

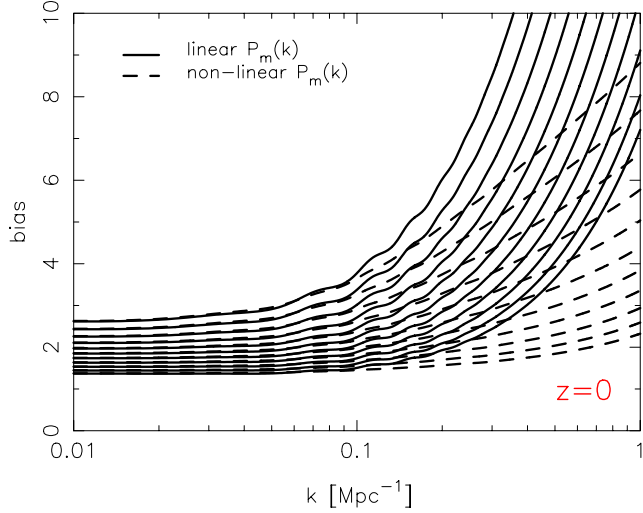


FIG. 12.— Nonlinear galaxy bias determined from the HOD emulator calculated using the linear  $P_m(k)$  (solid) and nonlinear  $P_m(k)$  (dashed) at  $z = 0$ . We have varied  $M_{cut}$  between the maximum and minimum parameter ranges to produce 10 different curves. The other HOD parameters are kept constant at the midpoint.

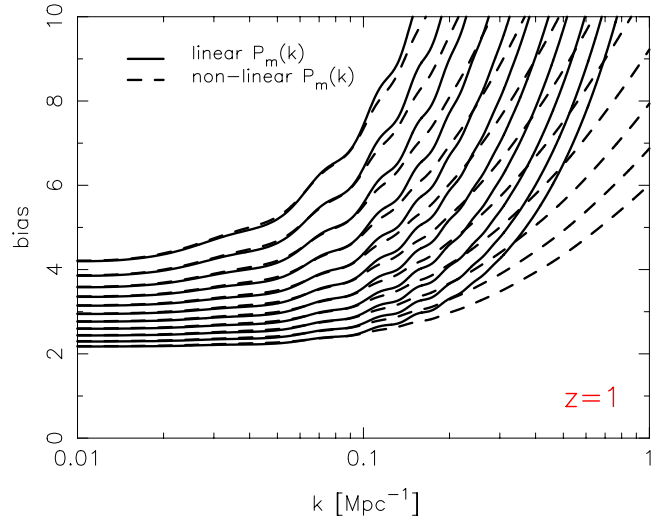


FIG. 13.— Galaxy bias as in Figure 12, but at  $z = 1$ .

## 8. CONCLUSIONS

We present an emulator for an HOD-based galaxy power spectrum obtained from an N-body simulation that is accurate to  $\sim 3\%$  over the range  $0.01 \leq k \leq 1 \text{ Mpc}^{-1}$  from  $0 \leq z \leq 1$ . Using our emulator, we explore the parameter degeneracies of the

five-parameter HOD model of Zheng et al. (2009), finding significant degeneracies between the parameters on large scales. Changes in  $M_{cut}$  dominate both the shape and overall amplitude of the HOD power spectrum, while the parameter  $\kappa$  has a very small effect on it. We also demonstrate how the emulator can be used to extract scale-dependent galaxy bias.

Emulation is a powerful technique for efficiently generating accurate models for highly nonlinear quantities in cosmology, such as the galaxy power spectrum. The emulator only requires a small number (100) models to be directly computed from the halo catalog of an N-body simulation, following which each prediction from the emulator takes less than a second. This can substantially reduce the run time needed for an MCMC analysis where, in the current approach e.g. White et al. (2011); Parejko et al. (2013), the halo catalog and power spectrum are recomputed at each step. To facilitate use by the community, the emulator code has been publicly released.

Future plans to extend the emulator include the addition of cosmological parameters to the HOD parameter space and the modeling of redshift space distortions.

## 9. ACKNOWLEDGMENTS

JK thanks Dave Higdon, Earl Lawrence and Amol Upadhye for useful discussions. Partial support for JK and KH was provided by NASA. NF and SH acknowledge partial support from the Scientific Discovery through Advanced Computing (SciDAC) program funded by the U.S. Department of Energy, Office of Science, jointly by Advanced Scientific Computing Research and High Energy Physics.

This research used resources of the Argonne Leadership Computing Facility (ALCF) under a Mira Early Science Project program. The ALCF is supported by DOE/SC under contract DE-AC02-06CH11357. Some of the work was conducted at the National Energy Research Scientific Computing Center, which is supported by the Office of Science of the U.S. Department of Energy under Contract No. DE-AC02-05CH11231.

The submitted manuscript has been created by UChicago Argonne, LLC, Operator of Argonne National Laboratory (“Argonne”). Argonne, a U.S. Department of Energy Office of Science laboratory, is operated under Contract No. DE-AC02-06CH11357. The U.S. Government retains for itself, and others acting on its behalf, a paid-up nonexclusive, irrevocable worldwide license in said article to reproduce, prepare derivative works, distribute copies to the public, and perform publicly and display publicly, by or on behalf of the Government.

## REFERENCES

Anderson, L., et al. 2012, MNRAS, 427, 3435

Baugh, C.M. 2006, Rep. Prog. Phys., 69, 3101

Baugh, C.M. 2013, PASA, 30, e030; arXiv:1302.2768 [astro-ph.CO]

Benson, A.J., Cole, S., Frenk, C.S., Baugh, C.M., & Lacey, C.G. 2000, MNRAS, 311, 793

Benson, A.J., Bower, R.G., Frenk, C.S., Lacey, C.G., Baugh, C.M., & Cole, S. 2003, ApJ, 599, 38

Benson, A.J. 2010, Phys. Rep., 495, 33

Berlind, A.A. & Weinberg, D.H. 2002, ApJ, 575, 587

Bhattacharya, S., et al. 2013, ApJ, 766, 32

Blake, C., Collister, A., & Lahav, O. 2008, MNRAS, 385, 1257

Brown, M.J.I., Zheng, Z., White, M., Dey, A., Jannuzzi, B.T., Benson, A.J., Brand, K., Brodwin, M., & Croton, D.J. 2008, ApJ, 682, 937

Cole, S., Aragon-Salamanca, A., Frenk, C.S., Navarro, J.F., & Zepf, S.E. 1994, MNRAS, 271, 781

Cole, S., et al. 2005, MNRAS, 362, 505

Conroy, C., Wechsler, R.H., & Kravtsov, A.V. 2006, ApJ, 647, 201

Cooray, A. & Sheth, R. 2002, Phys. Rep., 372, 1

Davis, M., Efstathiou, G., Frenk, C., & White, S.D.M. 1985, ApJ, 292, 371

Dekel, A. & Rees, M.J. 1987, Nature 326, 455

Einasto, J., Klypin, A.A., Saar, E., & Shandarin, S.F. 1984, MNRAS, 206, 529

Eisenstein, D.J., et al. 2005, ApJ, 633, 560

Gao, L., Springel, V., & White, S.D.M. 2005, MNRAS, 363, L66

Guo, Q., White, S., Cheng, L., & Bolyan-Kolchin, M. 2010, MNRAS, 404, 1111

Habib, S., Heitmann, K., Higdon, D., Nakhleh, C., & Williams, B. 2007, Phys. Rev. D 76, 083503

Habib, S., Pope, A., Lukic, Z., Daniel, D., Fasel, P., Desai, N., Heitmann, K., Hsu, C.-H., Ankeny, L., Mark G., Bhattacharya, S., & Ahrens, J. 2009, J. Phys. Conf. Ser., 180, 012019

Habib, S., Morozov, V., Finkel, H., Pope, A., Heitmann, K., Kumaran, K., Peterka, T., Insley, J., Daniel, D., Fasel, P., Frontiere, N., & Lukic, Z. 2012, arXiv:1211.4864 [cs.DC]

Heitmann, K., Higdon, D., Nakhleh, C., & Habib, S. 2006, ApJ, 646, L1

Heitmann K., Higdon D., White M., Habib S., Williams, B.J., & Wagner, C. 2009, ApJ, 705, 156

Heitmann K., White M., Wagner C., Habib S., & Higdon D. 2010, ApJ, 715, 104

Heitmann, K., Lawrence, E., Kwan, J., Habib, S., & Higdon, D. 2013; arXiv:1304.7849 [astro-ph.CO]

Jing, Y.P., Mo H.J., & Börner, G. 1998, ApJ, 494, 1

Kauffmann, G., White, S.D.M., & Guiderdoni, B. 1993, MNRAS, 264, 201

Kauffmann, G., Nusser, A., & Steinmetz, M. 1997, MNRAS, 286, 795

Kaiser, N. 1984, ApJ, 284, L9

Kulkarni, G.V., Nichol, R.C., Sheth, R.K., Seo H.-J., Eisenstein, D.J., & Gray, A. 2007, MNRAS, 378, 1196

Kwan, J., Bhattacharya, S., Heitmann, K., & Habib, S. 2013, ApJ, 768, 123

Lawrence, E., Heitmann, K., White M., Higdon D., Wagner C., Habib S., & Williams, B. 2010, ApJ, 713, 1322

Lukic, Z., et al. 2007, ApJ, 671, 1160

McDonald, P. 2006, Phys. Rev. D, 74, 103512

McDonald, P. 2006, Phys. Rev. D, 74, 129901

Moster, B.P., Somerville, R.S., Maulbetsch, C., van den Bosch, F.C., Maccio, A.V., Naab, T., & Oser, L. 2010, ApJ, 710, 903

Padmanabhan, N., White, M., Norberg, P., & Porciani, C., 2009, MNRAS, 397, 1862

Parejko, J.K., et al. 2013, MNRAS, 428, 98

Parkinson, D., et al. 2012, Phys. Rev. D, 86, 103518

Peacock, J.P., & Smith, R.E. 2000, MNRAS, 318, 1144

Phleps, S., Peacock, J.A., Meisenheimer, K., & Wolf, C., 2006, A&A, 457, 145

Pope, A.C., et al. 2004, ApJ, 607, 655

Pope, A., Habib, S., Lukic, Z., Daniel, D., Fasel, P., Desai, N., & Heitmann, K. 2010, Comp. Sci. & Eng. 12, 17

Reid, B.A., et al. 2012, MNRAS, 426, 2719

Seljak, U. 2000, MNRAS, 318, 203

Somerville, R.S., & Primack, J.R. 1999, MNRAS, 310, 1087

Swanson, M. E. C., Percival, W. J. & Lahav, O. 2010, MNRAS, 409, 1100

Tinker, J., et al., 2010, ApJ, 724, 878

Tegmark, M. 1997, Phys. Rev. Lett. 79, 3806

Tegmark, M., et al. 2004, ApJ, 606, 702

Tegmark, M., et al. 2006, Phys. Rev. D, 74, 123507

Vale, A. & Ostriker, J.P. 2004, MNRAS, 353, 189

Wake, D.A., et al. 2008, MNRAS, 387, 1045

Wetzel, A.R., & White, M. 2010, MNRAS, 403, 1072

White, M., et al. 2011, ApJ, 728, 126

White, S.D.M., & Frenk, C.S. 1991, ApJ, 379, 52

Zehavi, I. et al. 2004, ApJ, 608, 16

Zehavi, I. et al. 2005, ApJ, 630, 1

Zheng, Z. 2004, ApJ, 610, 61

Zheng, Z., et al. 2005, ApJ, 633, 791

Zheng, Z., Zehavi, I., Eisenstein, D.J.; Weinberg, D.H., & Jing, Y.P. 2009, ApJ, 707, 554